Interaction of Phosphonate Analogues of the Tetrahedral Reaction Intermediate with 5-Enolpyruvylshikimate-3-phosphate Synthase in Atomic Detail[†,‡]

Melanie A. Priestman,[§] Martha L. Healy,[§] Andreas Becker,[§] David G. Alberg,[||] Paul A. Bartlett,[||] Gerald H. Lushington,[⊥] and Ernst Schönbrunn*[,§]

Department of Medicinal Chemistry and Molecular Graphics and Modeling Laboratory, University of Kansas, Lawrence, Kansas 66045, and Department of Chemistry, University of California, Berkeley, California 94720-1460

Received August 19, 2004; Revised Manuscript Received November 12, 2004

ABSTRACT: The enzyme 5-enolpyruvylshikimate-3-phosphate synthase (EPSPS) catalyzes the penultimate step of the shikimate pathway and is the target of the broad-spectrum herbicide glyphosate. Since the functionality of the shikimate pathway is vital not only for plants but also for microorganisms, EPSPS is considered a prospective target for the development of novel antibiotics. We have kinetically analyzed and determined the crystal structures of *Escherichia coli* EPSPS inhibited by (*R*)- and (*S*)-configured phosphonate analogues of the tetrahedral reaction intermediate. Both diastereomers are competitive inhibitors with respect to the substrates of the EPSPS reaction, shikimate-3-phosphate (S3P) and phosphoenolpyruvate (PEP). Remarkably, the (*S*)-phosphonate (K_{iS3P} = 750 nM), whose configuration corresponds to that of the genuine tetrahedral intermediate, is a much weaker inhibitor than the (*R*)-phosphonate analogue (K_{iS3P} = 16 nM). The crystal structures of EPSPS liganded with the (*S*)- and (*R*)-phosphonates, at 1.5 and 1.9 Å resolution, respectively, revealed that binding of the (*R*)-phosphonate induces conformational changes of the strictly conserved residues Arg124 and Glu341 within the active site. This appears to give rise to substantial structural alterations in the amino-terminal globular domain of the enzyme. By contrast, binding of the (*S*)-phosphonate renders the enzyme structure unchanged. Thus, EPSPS may facilitate the tight binding of structurally diverse ligands through conformational flexibility. Molecular docking calculations did not explain why the (*R*)-phosphonate is the better inhibitor. Therefore, we propose that the structural events during the open−closed transition of EPSPS are altered as a result of inhibitor action.

5-enolpyruvylshikimate-3-phosphate synthase (EPSPS; EC 2.5.1.19) is the sixth enzyme of the shikimate pathway, which is essential for the synthesis of aromatic amino acids and of almost all other aromatic compounds in plants, fungi, and microoroganisms (*1*−*3*), including apicomplexan parasites (*4*). EPSPS has been extensively studied over the last three decades, since it was identified as the target of glyphosate, the active ingredient of Monsanto's broad-spectrum herbicide Roundup (*5*). Because the shikimate pathway is absent from mammals but essential for the pathogenesis of a number of microorganisms, enzymes of this pathway have received considerable attention recently as potential antimicrobial targets (*6*−*8*). The following findings in particular, indicate the importance of functional EPSPS for microbial survival: (i) deletion of the *aroA* gene, which encodes EPSPS, causes *Streptomyces pneumoniae* strains and *Bordetella bronchiseptica* to be attenuated for virulence (*6*, *9*), (ii) the growth of *Mycobacterium* depends on the functionality of the shikimate pathway (*10*), and (iii) glyphosate restricts the growth of *Thermotoga gondii* (*4*). Recently, it has been suggested that the shikimate pathway also presents an attractive target for malaria chemotherapy because shikimate analogues have been shown to inhibit the growth of *Plasmodium falciparum* (*11*).

EPSPS catalyzes the transfer of the enolpyruvyl moiety of phosphoenol pyruvate (PEP)[1] to the 5-hydroxyl of shikimate-3-phosphate (S3P) (Figure 1). The reaction is chemically unusual, since it proceeds via C−O bond cleavage of PEP rather than via P−O bond cleavage as is the case in most PEP-utilizing enzymes. The overall enolpyruvyl transfer reaction is an addition−elimination process in which the PEP molecule is covalently added to a target hydroxyl, forming a tetrahedral intermediate (TI) (*12*, *13*) before inorganic phosphate (P_i) is released to yield the enolpyruvyl product. The only other enzyme known to catalyze enolpyruvyl transfer is MurA, the first enzyme of bacterial cell wall biosynthesis, which is the target of the broad-spectrum antibiotic fosfomycin. Structural studies of *Escherichia coli* EPSPS revealed that the enzyme exists in an open, unliganded state (*14*) and a closed, S3P-liganded state (*15*) or

[†] This work was supported by the NIH Center of Biomedical Research Excellence (P20 RR16443-01).

[‡] The atomic coordinates and structure factors of *E. coli* EPSPS liganded with the (*S*)- and (*R*)-phosphonate TI analogues have been deposited with the Protein Data Bank (accession codes 1X8R and 1X8T, respectively).

* Corresponding author: Department of Medicinal Chemistry, University of Kansas, 4040a Malott Hall, Lawrence, KS 66045. E-mail eschoenb@ku.edu; phone 785-864-4503; fax 785-864-5326.

[§] Department of Medicinal Chemistry, University of Kansas.

[||] University of California.

[⊥] Molecular Graphics and Modeling Laboratory, University of Kansas.

[1] [1]Abbreviations: EPSP, 5-enolpyruvylshikimate-3-phosphate; PEP, phosphoenolpyruvate; S3P, shikimate-3-phosphate; TI, tetrahedral intermediate.

10.1021/bi048198d CCC: $30.25
Published on Web 02/10/2005

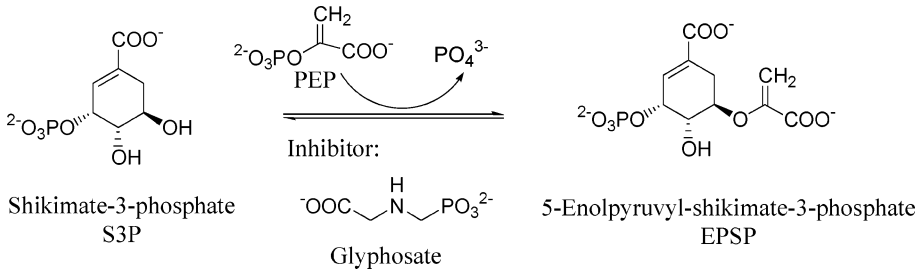

FIGURE 1: Reaction catalyzed by EPSPS.

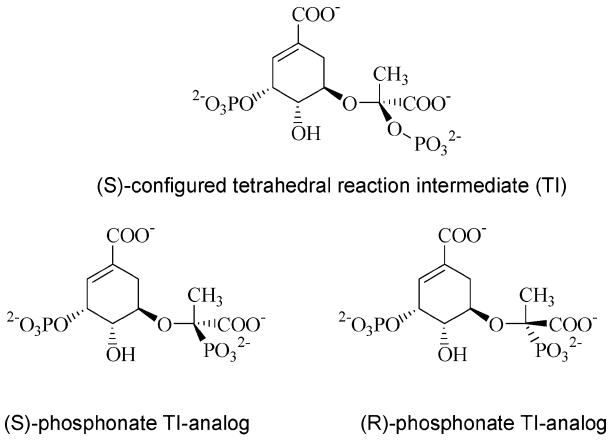

FIGURE 2: Configuration of the genuine tetrahedral reaction intermediate (TI) and the phosphonate TI analogues probed in this work.

TI-liganded state (*16*), indicating that the enolpyruvyl transfer reaction follows an induced-fit mechanism. The second substrate, PEP, and the inhibitor glyphosate bind to the closed state of the enzyme, adjacent to the target hydroxyl group of S3P (*15*). Recent work on *S. pneumoniae* EPSPS has confirmed these distinct structural features (*17*).

Several inhibitors of EPSPS have been reported in the literature. All of these were ground-state, reaction intermediate-state, or glyphosate analogues. While these inhibitors have been characterized kinetically, atomic structure information of inhibited EPSPS is still limited to the dead-end complex with glyphosate (*15*, *17*). The most potent EPSPS inhibitors discovered to date are analogues of the TI. Among these are the (*R*)- and (*S*)-phosphonate TI analogues (Figure 2), which were kinetically characterized for the reverse reaction of EPSPS from *Petunia hybrida* (*18*, *19*). Because the (*R*)-diastereomer was the more potent inhibitor, it was concluded at that time that the configuration at the C atom of PEP in the genuine TI is (*R*). However, recent crystallographic and chemical studies demonstrated that the genuine TI of the EPSPS reaction is (*S*)-configured (*16*, *20*). Further analysis of these TI analogues by stopped-flow fluorescence kinetics revealed that the off rates of the interaction of the genuine TI and both phosphonate analogues with *E. coli* EPSPS were similar, while the on rates differed drastically (*21*). These authors suggested that the slow onset of binding of the analogues might reflect significant structural changes to accommodate both analogues in binding to the enzyme. Thus, the rationale for the potent inhibition of EPSPS by the (*R*)-phosphonate TI analogue has remained obscure.

Here, we have determined the high-resolution structures of the (*R*)- and (*S*)-phosphonate TI analogues in complex with *E. coli* EPSPS. While the interaction of the (*S*)-phosphonate with EPSPS is similar to that observed for the genuine TI and the ternary complex with S3P and glyphosate, the (*R*)-phosphonate induces substantial conformational changes in the enzyme. Thus, the potent inhibition of EPSPS by the (*R*)-phosphonate appears to be the result of the enzyme's conformational flexibility to accommodate inhibitor binding. Such structural changes have never been observed with liganded EPSPS and are not predictable with molecular docking programs. The implications from these studies for the design of novel inhibitors targeting EPSPS are discussed.

MATERIALS AND METHODS

S3P (triethylammonium salt) was synthesized from shikimic acid by use of recombinant archaeal shikimate kinase (*22*), and purified via anion-exchange chromatography on Q-Sepharose. Syntheses of the (*R*)- and (*S*)-phosphonate TI analogues were reported previously (*18*, *19*). PEP (potassium salt) and all other chemicals were purchased from Sigma (St. Louis, MO) unless otherwise noted. The Pierce (Rockford, IL) Coomassie reagent with bovine serum albumin as a standard was used to determine protein concentrations.

Overexpression and Purification of EPSPS. E. coli EPSPS in a pET 24d vector (Novagen, Madison, WI) was transformed and overexpressed in BL21 DE3 competent cells (Stratagene, La Jolla, CA). EPSPS was purified at 4 °C with an ÄKTA fast protein liquid chromatography (FPLC) system (Amersham Biosciences, Piscataway, NJ) by hydrophobic exchange on phenyl-Sepharose [1−0 M $(NH_4)_2SO_4$] and anion exchange on Q-Sepharose (0−0.4 M KCl). The buffer was 50 mM Tris-HCl, pH 7.8, including 1 mM dithiothreitol (DTT) and 1 mM ethylenediaminetetraacetic acid (EDTA). Purified enzyme was desalted, concentrated to 100 mg/mL, and stored at −80 °C.

Inhibition Kinetics. The activity of EPSPS was assayed in 100 μL of 50 mM HEPES-NaOH, pH 7.0, and 2 mM DTT at 20 °C by determining the amount of inorganic phosphate produced in the reaction (*23*). The reaction was started by addition of EPSPS. The enzyme was allowed to react for 3 min before the Lanzetta reagent (800 μL) was added, thereby stopping the reaction. Color development was stopped after 5 min by addition of 100 μL of 34% (w/v) sodium citrate. Change in optical density was measured at 660 nm and the amount of inorganic phosphate was determined by comparison to phosphate standards. Enzyme activity is expressed as micromoles of phosphate produced per minute of reaction time per milligram of enzyme (units per milligram). The final concentration of enzyme in the assay mixture was about 22 nM for all assays. Data evaluation was performed with SigmaPlot (SPSS Science, Chicago, IL).

Table 1: Summary of Data Collection and Structure Refinement[a]

data set	EPSPS·(*S*)-phosphonate	EPSPS·(*R*)-phosphonate
space group	$P2_12_12_1$	$P2_12_12_1$
unit cell dimensions (Å)	$a = 57.7$, $b = 85.2$, $c = 87.5$	$a = 57.2$, $b = 84.5$, $c = 99.2$
angles (deg)	$\alpha = \beta = \gamma = 90$	$\alpha = \beta = \gamma = 90$
molecules/asymmetric unit	1	1
protein atoms	3232	3232
alternate atom positions	46	45
ligand atoms	25	25
solvent molecules	568	468
formate ions	12	7
rmsd[b] bonds (Å)	0.009	0.007
rmsd angles (deg)	1.56	1.46
resolution range (Å)	10.0−1.5 (1.6−1.5)	10.0−1.9 (2.0−1.9)
measured reflections	450 255 (66 502)	219 201 (29 717)
unique reflections	66 430 (11 149)	33 201 (4569)
completeness (%)	95.3 (92.1)	96.6 (94.9)
$I/\sigma I$	18.3 (7.1)	16.6 (8.0)
R_{mrgd-F}[c] (%)	4.8 (14.3)	5.6 (1.43)
R_{meas}[c] (%)	6.5 (27.3)	8.9 (27.1)
R_{cryst}[d] (%)	16.8	16.3
R_{free}[e] (%)	19.5	20.7

[a] Values in parentheses refer to the highest resolution shell. [b] Rmsd, root-mean-square deviation from ideal values. [c] R_{meas} and R_{mrgd-F} as defined by Diederichs and Karplus (*28*) are quality measures of the individual intensity observations and the reduced structure factor amplitudes, respectively. [d] $R_{cryst} = 100\ \Sigma|F_{obs} - F_{model}|/\Sigma F_{obs}$, where F_{obs} and F_{model} are observed and calculated structure factor amplitudes. [e] R_{free} is R_{cryst} calculated for randomly chosen unique reflections that were excluded from the refinement [1329 for EPSPS·(*S*)-phosphonate and 1162 for EPSPS·(*R*)-phosphonate, respectively].

IC_{50} values were determined by fitting data to

$$v = V_{min} + \frac{V_{max} - V_{min}}{1 + \left(\frac{[I]}{IC_{50}}\right)^n} \quad (1)$$

where v is the initial velocity, V_{max} is the maximum velocity, V_{min} is the minimum velocity, [I] is the phosphonate inhibitor concentration, and n is the Hill slope.

For determination of the K_i values, enzyme activities at increasing S3P, PEP, and inhibitor concentrations were recorded, and the data were fit to the Michaelis−Menten equation:

$$v = \frac{V_{max}[S]}{K_{m(obs)} + [S]} \quad (2)$$

where v is the initial velocity, V_{max} is the maximum velocity, $K_{m(obs)}$ is the observed Michaelis constant, and [S] is the substrate concentration.

The K_i values for the (*S*)- and (*R*)-phosphonate analogues were determined by linear regression of the replot of the $K_{m(obs)}$ values versus the concentration of the inhibitor [I]:

$$K_{m(obs)} = \left(\frac{K_m}{K_i}\right)[I] + K_m \quad (3)$$

where K_m is the true Michaelis constant and K_i is the inhibition constant. Possible time-dependent inhibition was accounted for by assaying EPSPS preincubated with the inhibitors prior to starting the reaction by the addition of substrates.

Crystallography. For crystallization, EPSPS was concentrated to 100 mg/mL on Centricon 30 devices (Amicon) at 4 °C. Crystals were grown at 19 °C in hanging droplets from 2.5 M sodium formate solutions in the presence of 10 mM (*S*)- or (*R*)-phosphonate analogue. Diffraction data were recorded at −180 °C by the rotation method on single flash-frozen crystals of EPSPS liganded with the (*S*)- or (*R*)-phosphonate analogue [detector, R-axis IV^{2+} image plate; X-rays, Cu Kα, focused by mirror optics; generator, Rigaku RU300 (MSC, The Woodlands, TX)]. The data were reduced with XDS (*24*). The program package CNS (*25*) was employed for phasing and refinement; model building was performed with O (*26*). The structures were solved by molecular replacement with wild-type EPSPS [PDB code 1G6S (*15*)] stripped of solvent molecules, ions, and ligands as search model. Refinement was performed by use of data to highest resolution with no σ cutoff applied. Several rounds (nine for R-EPSPS and eight for S-EPSPS) of minimization, simulated annealing (2500 K starting temperature) and restrained individual *B*-factor refinement were carried out. The (*S*)- and (*R*)-phosphonate analogues were modeled unambiguously into the electron density map (Figure 6). Data collection and refinement statistics are summarized in Table 1. Figures 7 and 8 were drawn with Molscript and Raster3D (*27*, *28*), Figure 6 with Bobscript (*29*) and Raster3D.

Molecular Docking. In silico docking experiments have been carried out to evaluate the relative energetics of the three ligands of interest, the genuine tetrahedral intermediate and its (*R*)- and (*S*)-phosphonate analogues, binding to different observed conformations of the EPSPS receptor. Specifically, they were docked, via AutoDock (*30*), to receptor models constructed from crystal structures corresponding to the EPSPS·TI (*16*), EPSPS·(*S*)-phosphonate (this work), and EPSPS·(*R*)-phosphonate (this work) complexes. Partial atomic charges for both the ligand and receptor models were generated according to the Gasteiger−Marsili formalism (*31*). Since the ligand carboxy moieties are observed to couple directly with arginine forks (each oxygen bound to an equivalent H-bond donor), we assumed charge delocalization across the oxygens (formal charge of −0.5 for each) when setting up the charge calculation. However, localized charges were used for ligand phosphate/phosphonate groups (two oxygens with formal −1 charges, one

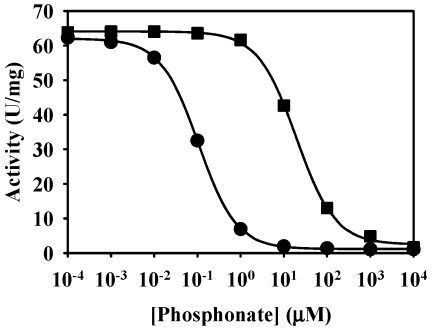

FIGURE 3: IC_{50} determination of the phosphonate TI analogues. EPSPS was assayed with 2.5 mM S3P and 2.5 mM PEP and increasing concentrations of the (*R*)- (●) or the (*S*)-phosphonate (■). Data were fit to eq 1, yielding IC_{50} values of 0.11 ± 0.002 μM for the (*R*)-phosphonate and 20 ± 1.1 μM for the (*S*)-phosphonate.

oxygen formally neutral) to accommodate inequivalently polarizing environments for different oxygen orientations.

RESULTS AND DISCUSSION

Inhibition Kinetics. Both the (*R*)- and (*S*)-phosphonate analogues of the genuine TI are rapidly reversible inhibitors of the forward reaction of *E. coli* EPSPS; incubation of the enzyme with either analogue does not result in time-dependent inhibition (data not shown). The IC_{50} values are 0.11 μM for the (*R*)-phosphonate and 20 μM for the (*S*)-phosphonate under saturating substrate concentrations (Figure 3). We have analyzed the steady-state inhibition kinetics of these TI analogues on the forward reaction of the enzyme. As expected from their structural similarity to the genuine TI (Figure 2), both diastereomers are competitive inhibitors with respect to S3P and PEP (Figures 4 and 5). The K_i values of the (*R*)-phosphonate are 16 nM and 24 nM for S3P and PEP, respectively. The K_i values of the (*S*)-phosphonate are 0.75 μM and 2.9 μM for S3P and PEP, respectively. The $K_{i(S3P)}$ values of both analogues are similar to the K_i values with respect to EPSP when EPSPS was assayed in the backward reaction (*18*). Thus, the (*R*)-phosphonate is the second most potent inhibitor of the EPSPS reaction reported to date [the (*R*)-difluoromethyl TI analogue inhibits EPSPS with a K_i of 4 nM (*19*)]. Remarkably, it is also a much stronger inhibitor than the (*S*)-phosphonate.

The action of these diastereomers was previously investigated by stopped-flow intrinsic fluorescence experiments, revealing that both analogues bind 2−4 orders of magnitude more slowly and perhaps more weakly to the enzyme as compared to the genuine TI (*21*). While the off rates of the interaction of EPSPS with the genuine TI and both analogues were similar, the on rate was ca. 300 times smaller with the (*R*)-phosphonate and ca. 18 000 times smaller with the (*S*) isomer. Recently, the absolute configuration of the genuine TI was assigned (*S*), by chemical (*20*) and crystallographic (*16*) studies. Thus, one intuitively would expect the (*S*)-phosphonate analogue to be the better inhibitor. Therefore, we determined the crystal structures of EPSPS bound with these analogues.

Enzyme−Inhibitor Complexes. The EPSPS·(*S*)-phosphonate (S-EPSPS) and EPSPS·(*R*)-phosphonate (R-EPSPS) structures were determined at 1.5 and 1.9 Å resolution, respectively (Table 1). The electron density around either ligand bound to the active site was unambiguous (Figure 6).

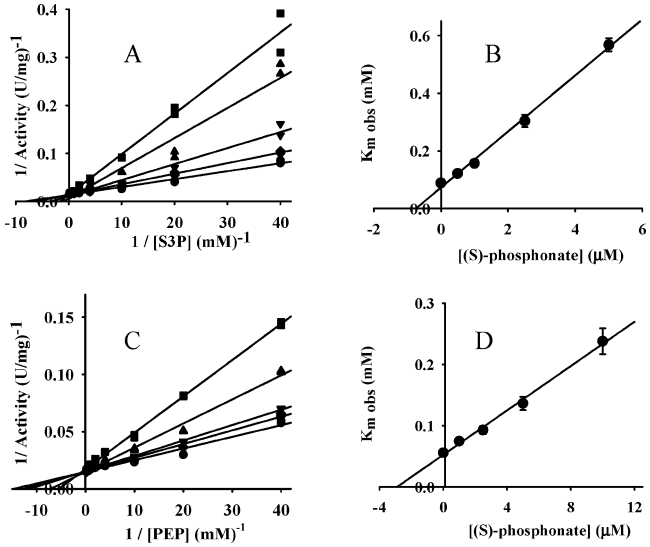

FIGURE 4: Steady-state kinetics of EPSPS inhibition by the (*S*)-phosphonate TI analogue. (A) Lineweaver−Burk presentation of EPSPS activity as a function of S3P and increasing (*S*)-phosphonate concentrations: 0 (●), 0.5 (◆), 1 (▼), 2.5 (▲), and 5 μM (■). The concentration of PEP was 2.5 mM. Data were fit to eq 2. (B) Replot of the observed K_ms obtained from panel A as a function of (*S*)-phosphonate concentration. Data were fit to eq 3, yielding a K_i of 0.75 ± 0.03 μM. (C) Lineweaver−Burk presentation of EPSPS activity as a function of PEP and increasing (*S*)-phosphonate concentrations: 0 (●), 1 (◆), 2.5 (▼), 5 (▲), and 10 μM (■). The concentration of S3P was 2.5 mM. Data were fit to eq 2. (D) Replot of the observed K_ms obtained from panel C as a function of (*S*)-phosphonate concentration. Data were fit to eq 3, yielding a K_i of 2.9 ± 0.12 μM.

The overall S-EPSPS structure is not changed when compared with the structure of the genuine TI state (Figure 7). With the exception of Glu341, which adopts a slightly different conformation to accommodate the carboxyl group of the (*S*)-phosphonate, all the residues around the PEP binding site remain essentially unchanged. Moreover, the hydrogen-bonding interaction pattern of the (*S*)-phosphonate with these residues is almost identical to that of the genuine TI, except for the missing interaction with Arg386, a strictly conserved residue in EPSPS. On the other hand, the (*S*)-phosphonate gains one hydrogen bond through interaction with the imidazole ring of His385, which is not the case for the genuine TI.

By contrast, gross changes in the enzyme structure occur as a result of binding of the (*R*)-phosphonate to EPSPS. In the active site, the side chains of residues Arg124 and Glu341, both strictly conserved in all EPSPS, undergo drastic conformational changes (Figure 7). The Glu341 side chain turns down as a result of steric clashes between its carboxyl group and one of the oxygen atoms of the phosphono group of the ligand. The Arg124 side chain appears to collapse because of the lack of negatively charged oxygen atoms to interact with. In all EPSPS structures known to date, the guanidinium group of Arg124 is involved in electrostatic interactions, namely, with the phosphonate group of glyphosate (*15*), the phosphate group of the genuine TI (*16*), and the phosphonate group of the (*S*)-phosphonate (Figure 7). These salt bridges appear to stabilize the Arg124 side chain, as reflected by the low temperature factors of 9−14 Å^2 in the aforementioned structures. By contrast, the temperature factor of the Arg124 guanidinium group in the R-EPSPS structure is about 40 Å^2, indicating a high degree

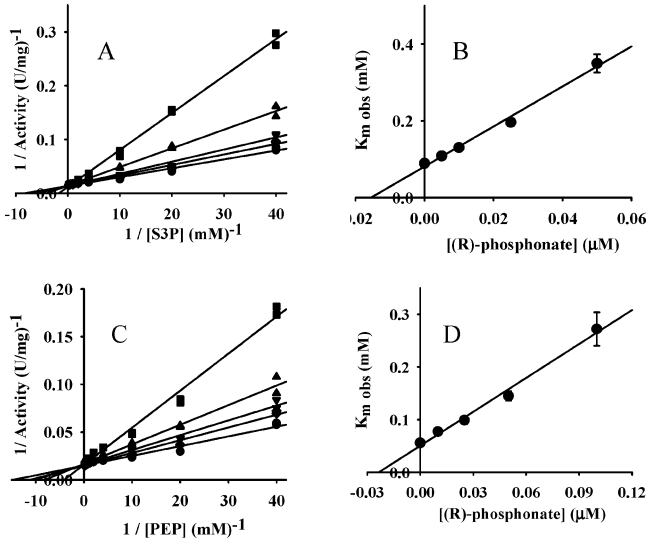

FIGURE 5: Steady-state kinetics of EPSPS inhibition by the (*R*)-phosphonate TI analogue. **(**A**)** Lineweaver−Burk presentation of EPSPS activity as a function of S3P and increasing (*R*)-phosphonate concentrations: 0 (●), 0.005 (◆), 0.01 (▼), 0.025 (▲), and 0.050 μM (■). The concentration of PEP was 2.5 mM. Data were fit to eq 2. **(**B**)** Replot of the observed K_ms obtained from panel A as a function of (*R*)-phosphonate concentration. Data were fit to eq 3, yielding a K_i of 0.016 ± 0.001 μM. **(**C**)** Lineweaver−Burk presentation of EPSPS activity as a function of PEP and increasing (*R*)-phosphonate concentrations: 0 (●), 0.01 (◆), 0.025 (▼), 0.05 (▲), and 0.1 μM (■). The concentration of S3P was 2.5 mM. Data were fit to eq 2. **(**D**)** Replot of the observed K_ms obtained from panel C as a function of (*R*)-phosphonate concentration. Data were fit to eq 3, yielding a K_i of 0.024 ± 0.001 μM.

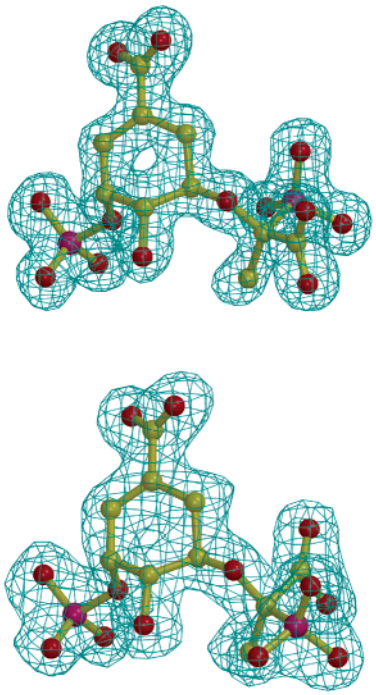

FIGURE 6: Crystallography of the phosphonate TI analogues bound to EPSPS. Displayed are the electron densities derived from $2F_o - F_c$ Fourier syntheses after the last refinement cycle, contoured at 1σ, for the (*S*)-phosphonate at 1.5 Å resolution (top) and the (*R*)-phosphonate at 1.9 Å resolution (bottom).

of flexibility, although the electron density of this residue is clearly visible. Apparently the carboxyl group of the ligand in the R-EPSPS complex is too far away from the guanidinium moiety of Arg124 to establish a salt bridge. It appears that this leads to the conformational change of the Arg124 side chain. The (*R*)-phosphonate-induced structural changes of Arg124 appear to extend to global changes in the N-terminal domain of EPSPS (the upper globular domain in Figure 8). It is unlikely that the conformational change of Glu341 contributes to these global changes as well, because its neighboring residues are not affected and because Glu341 belongs to the C-terminal domain (the bottom domain). Particularly affected is the region spanning residues 81−126, in which the backbone shifts by up to 2 Å (Figure 8). Some of the residues within this region undergo drastic conformational changes as well, for example, Asn94 and Arg120. Overall, the R-EPSPS exists in a slightly more open state than the S-EPSPS.

Why Is the "Wrong" Diastereomer the Better Inhibitor? Notably, neither the micro- nor the macroconformational changes induced by the (*R*)-phosphonate are observed with any of the other known liganded EPSPS structures. On the other hand, the (*S*)-phosphonate exerts essentially the same binding pattern in the active site as the genuine TI or the ternary complex with S3P and glyphosate. As envisioned (*21*), the "wrong" configuration of the TI analogue fits the active site, indeed. Apparently this is made possible because of structural changes within and around the active site, possibly necessary to accommodate the bulky phosphonate group in the binding pocket reserved for the carboxyl group of PEP. Molecular docking with the EPSPS·TI complex (*16*; PDB entry 1Q36) as the sole receptor structure revealed binding potentials in the order TI > (*S*)-phosphonate > (*R*)-phosphonate (Table 2). This order of binding and the binding energies remain the same when the S-EPSPS structure serves as receptor. Remarkably, binding of the TI to the R-EPSPS structure is less favored than that of both phosphonate analogues. On the other hand, all ligands, including the (*R*)-phosphonate, appear to bind more weakly to the R-EPSPS structure than to the other receptors, probably caused by the missing Arg124 and Glu341 side chains as binding partners (Figure 7). None of these calculations result in higher binding energies for the (*R*)-phosphonate as compared to the (*S*)-phosphonate. Thus, the mere knowledge of the interaction of these analogues with active-site residues appears to be insufficient to explain the high inhibitory potency of the (*R*)-phosphonate. Therefore, it is likely that the structural events that lead the formation of the active site are altered.

There is evidence that the transition from an open (unliganded) to a closed (substrate-liganded) EPSPS state is triggered by S3P and not by PEP (*15*−*17*). Similarly, the mechanistic and structural homologous enzyme MurA interacts with UNAG in its open form, which results in global structural changes leading to a closed form (*16*, *32*−*36*). For both enzymes, domain closure results in accumulation of positively charged side chains, originating from the N- and C-terminal globular domains (Figures 7 and 8), to which the anionic PEP molecule would bind, adjacent to the target hydroxyl of S3P or UNAG. This induced-fit mechanism requires the existence of a collision complex between S3P and the open enzyme form (Figure 9), possibly located at the N-terminal domain (*37*), but being substantially different from the active-site architecture. Given that entry and exit routes for S3P or EPSP do not exist in the closed enzyme state, it is likely that EPSPS has to undergo the open−closed transition with each catalytic cycle (Figure 9). Likewise, the

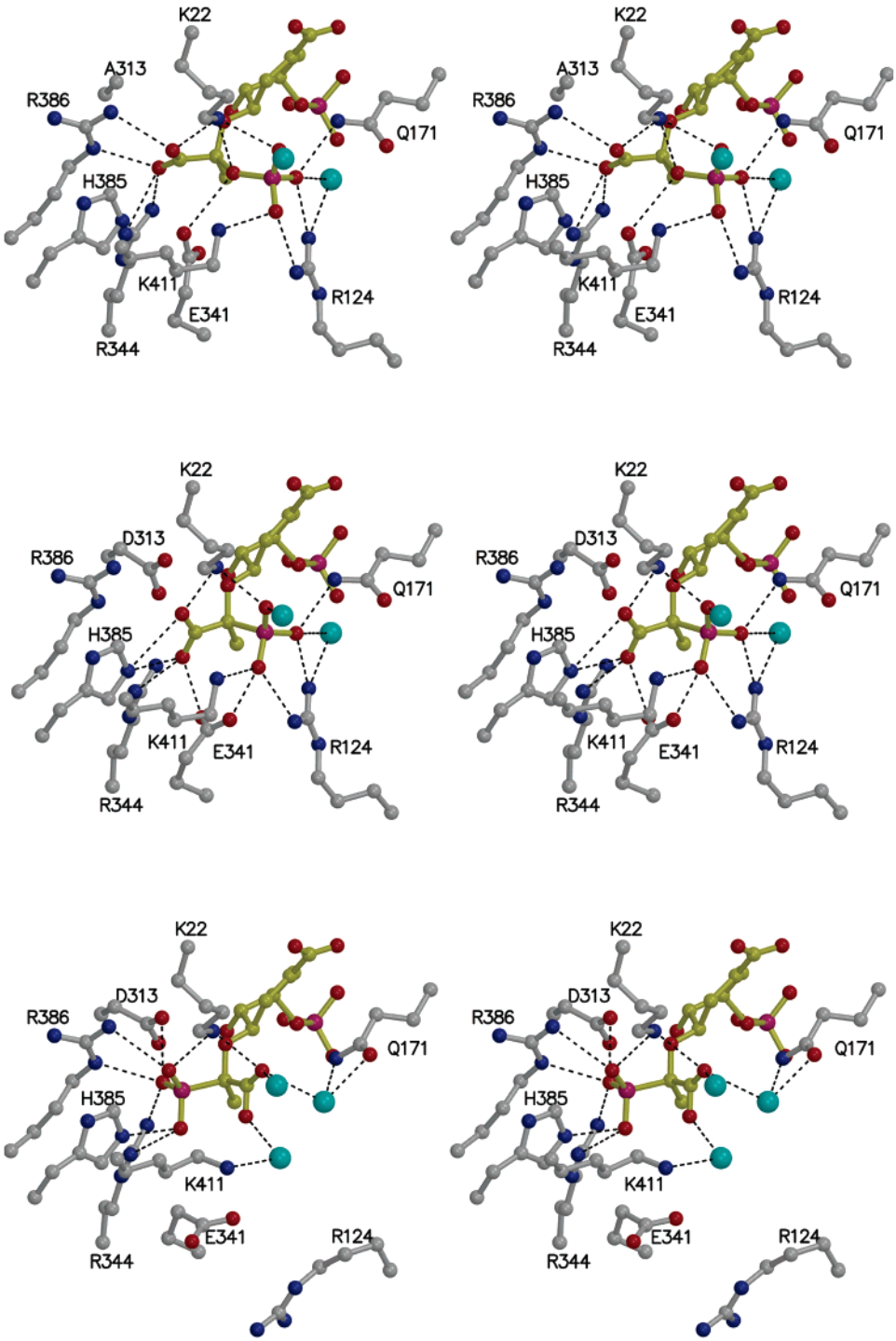

FIGURE 7: Comparison of the binding patterns for the genuine TI and the phosphonate analogues in EPSPS around the PEP site. Top stereopair: Genuine TI in the D313A EPSPS (*17*). Middle stereopair: (*S*)-Phosphonate in the wild-type EPSPS. Bottom stereopair: (*R*)-Phosphonate in the wild-type EPSPS. Polar or charged interactions are denoted by dashed lines. The models are color-coded according to atom types: carbon atoms of the respective ligands are shown in yellow, carbon atoms of the surrounding enzyme residues in gray, nitrogen atoms in blue, oxygen atoms in red, and phosphorus atoms in magenta. Turquoise balls designate water molecules.

TI or the phosphonate analogues will bind to the open enzyme form, inducing the transition to the closed state, and these molecules would only dissociate from the enzyme upon opening. Thus, the stopped-flow data utilizing intrinsic fluorescence changes (*21*) do not merely reflect k_{on} and k_{off} of the dissociation constant, $K_{d(TI)}$, but also the unimolecular rate constants, k_3^* and k_4^*, of the open−closed transition (Figure 9). In fact, Anderson and Johnson (*21*) observed complex biphasic kinetics with both analogues but not with the genuine TI, which was interpreted as "a rate-limiting isomerization of the enzyme analog complex". Such isomerization would be reflected by an altered ratio of k_3^* and k_4^* of Figure 9. Neither analogue is a slow-binding inhibitor, which is in accordance with the unchanged off-rates observed by Anderson and Johnson (*21*). If we assume that the rate-limiting steps of the interaction of the analogues with the enzyme indeed are k_3^* and k_4^* (and not k_1^* or k_2^* that determine the K_d), and furthermore that the off-rate (k_4^*) is unchanged, it would be k_3^* that varies as a function of the TI analogue structure. Consequently, the K_i is probably more

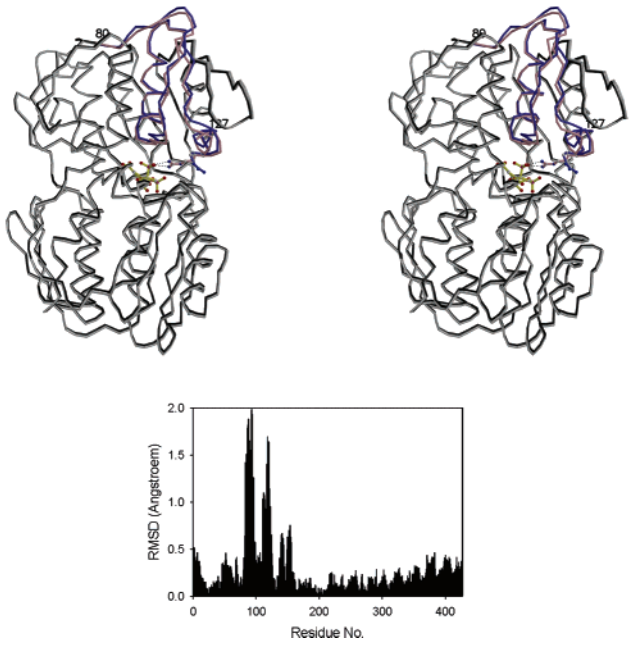

FIGURE 8: Global structural changes induced by the binding of the (*R*)-phosphonate TI analogue to EPSPS. Top: Stereopair of the Cα trace of EPSPS liganded with the (*S*)- and (*R*)-phosphonates (light gray and darker gray, respectively). The backbone structure remains unchanged for the bottom globular domain and most parts of the upper domain. Only the region spanning residues 81−126 shifts upon the conformational change of Arg124 (blue = S-EPSPS; pink = R-EPSPS). Shown in yellow is the (*S*)-phosphonate bound to the active site of S-EPSPS. Bottom: Root-mean-square deviation (rmsd) of the Cα positions of R-EPSPS backbone with respect to that of S-EPSPS.

Table 2: Docking Free Energies[a] for TI and the (*R*)- and (*S*)-Phosphonate Analogues into EPSPS

	EPSPS·TI[b]	S-EPSPS[c]	R-EPSPS[d]
TI	−19.25	−19.18	−15.43
(*S*)-phosphonate	−18.29	−18.48	−17.01
(*R*)-phosphonate	−17.89	−17.85	−17.04

[a] Docking free energies are given in kilocalories per mole. [b] Receptor = PDB entry 1Q36 (*16*). [c] Receptor = PDB entry 1X8R (this work). [d] Receptor = PDB entry 1X8T (this work).

accurately defined as $(k_2^* + k_3^*)/k_1^*$, in which the rate of the open−closed transition, k_3^*, may determine the tightness of ligand binding.

In the absence of structural data about the nature of the collision complex, we can only hypothesize that the phosphonate group in the (*R*)-isomer, positioned at the carboxyl site of the genuine TI, compensates for the "wrong" configuration, in that it triggers the open−closed transition more efficiently than the (*S*)-isomer. Because S3P alone induces the open−closed transition (*15*), the key element of the structural changes induced by both TI analogues is likely to be the S3P moiety. It is possible, however, that the attached PEP-like moieties influence this transition, presumably through electrostatic interactions of the carboxyl and phosphonate groups with enzyme residues that are important for the induced-fit mechanism but yet to be identified.

CONCLUSIONS

While atomic structures of medicinally important proteins are being determined at an ever-increasing rate, the translation of this information to the design of new drugs is often not as straightforward as was envisioned. For example, the structure of EPSPS in its dead-end complex with glyphosate was considered a breakthrough in the rational design of inhibitors for this enzyme (*7*). However, the results from this work demonstrate that the active site of EPSPS undergoes structural changes upon inhibitor binding on a scale that cannot be predicted by conventional computational methods. On the basis of the potent inhibition of EPSPS by the (*R*)-phosphonate TI analogue, it appears that this enzyme may facilitate the tight binding of structurally diverse ligands through conformational flexibility of its active site, and possibly altered kinetics of the open−closed transition. Thus, molecular docking with the presently known EPSPS structures is an incomplete approach to the design of novel inhibitors. As a consequence, more experimental data on the structure and dynamics of various EPSPS−ligand complexes are needed to more effectively apply structure-based drug design of this enzyme in the future.

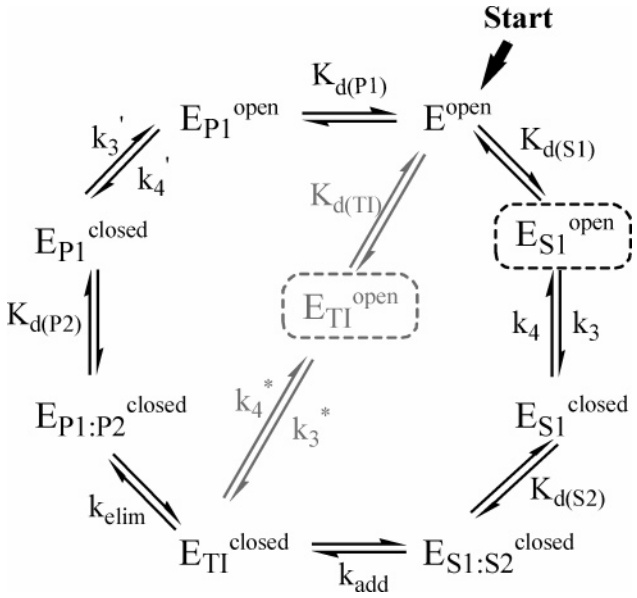

FIGURE 9: Proposed catalytic cycle for EPSPS. In the forward reaction, the unliganded, open form of EPSPS reacts with S3P (S1) to build up a rapidly reversible collision complex (E_{S1}^{open}), characterized by $K_{d(S1)}$. The collision complex undergoes a structural transition to the closed form (E_{S1}^{closed}), characterized by the unimolecular rate constants k_3 and k_4. The second substrate, PEP (S2), binds to the closed state, characterized by $K_{d(S2)}$, followed by the chemical reaction to yield the tetrahedral intermediate (E_{TI}^{closed}). The subsequent elimination step yields the products, EPSP (P1) and inorganic phosphate (P2). Phosphate release, characterized by $K_{d(P2)}$, precedes the closed-open transition, the latter characterized by the unimolecular rate constants k_3' and k_4', to allow release of EPSP, characterized by $K_{d(P1)}$. The pathway displayed diagonally across the cycle is that of the TI or phosphonate analogues interacting with the open enzyme, which is determined by a dissociation constant $K_{d(TI)}$ and the rate constants k_3^* and k_4^*. The unchanged off rates observed in the stopped-flow experiments by Anderson and Johnson (*21*) probably reflect k_4^*. This catalytic cycle is applicable to MurA, the other known enolpyruvyl transferase, too. Crystal structures of the following enzyme states are known (listed with PDB accession numbers): E^{open} [EPSPS, 1EPS and 1RF5 (*14*, *17*); MurA, 1NAW, 1EJC, and 1EJD (*32*, *35*)]; E_{S1}^{closed} [EPSPS, 1G6T (*15*); MurA, Schönbrunn, unpublished); E_{TI} [EPSPS, 1Q36 (*16*); MurA, 1Q3G (*16*)]; $E_{P1:P2}^{closed}$ [MurA, 1RYW (*38*)]; E_{P1}^{closed} [EPSPS, Schönbrunn, unpublished]. To date, the inhibited enzymes [EPSPS·S3P·glyphosate, 1G6S and 1RF6 (*15*, *17*); MurA·UNAG·fosfomycin, 1UAE (*33*)] may best represent the respective $E_{S1:S2}$ states.

ACKNOWLEDGMENT

We thank Todd Funke (University of Kansas) for help in enzyme purification and crystallization during his undergraduate studies.

REFERENCES

1. Bentley, R. (1990) The shikimate pathway—a metabolic tree with many branches, *Crit. Rev. Biochem. Mol. Biol. 25*, 307−384.
2. Haslam, E. (1993) *Shikimic acid: metabolism and metabolites*, John Wiley & Sons, Chichester, U.K.
3. Kishore, G. M., and Shah, D. M. (1988) Amino acid biosynthesis inhibitors as herbicides, *Annu. Rev. Biochem. 57*, 627−663.
4. Roberts, F., Roberts, C. W., Johnson, J. J., Kyle, D. E., Krell, T., Coggins, J. R., Coombs, G. H., Milhous, W. K., Tzipori, S., Ferguson, D. J., Chakrabarti, D., and McLeod, R. (1998) Evidence for the shikimate pathway in apicomplexan parasites, *Nature 393*, 801−805.
5. Steinrucken, H. C., and Amrhein, N. (1980) The herbicide glyphosate is a potent inhibitor of 5-enolpyruvyl-shikimic acid-3-phosphate synthase, *Biochem. Biophys. Res. Commun. 94*, 1207−1212.
6. McDevitt, D., Payne, D. J., Holmes, D. J., and Rosenberg, M. (2002) Novel targets for the future development of antibacterial agents, *J. Appl. Microbiol. 92*, 28S−34S.
7. Alibhai, M. F., and Stallings, W. C. (2001) Closing down on glyphosate inhibition—with a new structure for drug discovery, *Proc. Natl. Acad. Sci. U.S.A. 98*, 2944−2946.
8. Roberts, C. W., Roberts, F., Lyons, R. E., Kirisits, M. J., Mui, E. J., Finnerty, J., Johnson, J. J., Ferguson, D. J., Coggins, J. R., Krell, T., Coombs, G. H., Milhous, W. K., Kyle, D. E., Tzipori, S., Barnwell, J., Dame, J. B., Carlton, J., and McLeod, R. (2002) The shikimate pathway and its branches in apicomplexan parasites, *J. Infect. Dis. 185*, S25−S36.
9. McArthur, J. D., West, N. P., Cole, J. N., Jungnitz, H., Guzman, C. A., Chin, J., Lehrbach, P. R., Djordjevic, S. P., and Walker, M. J. (2003) An aromatic amino acid auxotrophic mutant of *Bordetella bronchiseptica* is attenuated and immunogenic in a mouse model of infection, *FEMS Microbiol. Lett. 221*, 7−16.
10. Parish, T., and Stoker, N. G. (2002) The common aromatic amino acid biosynthesis pathway is essential in *Mycobacterium tuberculosis*, *Microbiology 148*, 3069−3077.
11. McConkey, G. A. (1999) Targeting the shikimate pathway in the malaria parasite *Plasmodium falciparum*, *Antimicrob. Agents Chemother. 43*, 175−177.
12. Anderson, K. S., and Sikorski, J. A. (1988) Isolation and structural elucidation of the tetrahedral intermediate in the EPSP synthase enzymatic pathway, *J. Am. Chem. Soc. 110*, 6577−6579.
13. Anderson, K. S., Sikorski, J. A., and Johnson, K. A. (1988) A tetrahedral intermediate in the EPSP synthase reaction observed by rapid quench kinetics, *Biochemistry 27*, 7395−7406.
14. Stallings, W. C., Abdel-Meguid, S. S., Lim, L. W., Shieh, H. S., Dayringer, H. E., Leimgruber, N. K., Stegeman, R. A., Anderson, K. S., Sikorski, J. A., Padgette, S. R., and Kishore, G. M. (1991) Structure and topological symmetry of the glyphosate target 5-enolpyruvylshikimate-3-phosphate synthase: a distinctive protein fold, *Proc. Natl. Acad. Sci. U.S.A. 88*, 5046−5050.
15. Schonbrunn, E., Eschenburg, S., Shuttleworth, W. A., Schloss, J. V., Amrhein, N., Evans, J. N., and Kabsch, W. (2001) Interaction of the herbicide glyphosate with its target enzyme 5-enolpyruvylshikimate 3-phosphate synthase in atomic detail, *Proc. Natl. Acad. Sci. U.S.A. 98*, 1376−1380.
16. Eschenburg, S., Kabsch, W., Healy, M. L., and Schonbrunn, E. (2003) A new view of the mechanisms of UDP−*N*-acetylglucosamine enolpyruvyl transferase (MurA) and 5-enolpyruvylshikimate-3-phosphate synthase (AroA) derived from X-ray structures of their tetrahedral reaction intermediate states, *J. Biol. Chem. 278*, 49215−49222.
17. Park, H., Hilsenbeck, J. L., Kim, H. J., Shuttleworth, W. A., Park, Y. H., Evans, J. N., and Kang, C. (2004) Structural studies of *Streptococcus pneumoniae* EPSP synthase in unliganded state, tetrahedral intermediate-bound state and S3P-GLP-bound state, *Mol. Microbiol. 51*, 963−971.
18. Alberg, D. G., and Bartlett, P. A. (1989) Potent inhibition of 5-enolpyruvylshikimate-3-phosphate synthase by a reaction intermediate analogue, *J. Am. Chem. Soc. 11*, 2337−2338.
19. Alberg, D. G., Lauhon, C. T., Nyfeler, R., Fassler, A., and Bartlett, P. A. (1992) Inhibition of EPSP synthase by analogues of the tetrahedral intermediate and EPSP, *J. Am. Chem. Soc. 114*, 3535−3546.
20. An, M., Maitra, U., Neidlein, U., and Bartlett, P. A. (2003) 5-Enolpyruvylshikimate 3-phosphate synthase: chemical synthesis of the tetrahedral intermediate and assignment of the stereochemical course of the enzymatic reaction, *J. Am. Chem. Soc. 125*, 12759−12767.
21. Anderson, K. S., and Johnson, K. A. (1990) "Kinetic competence" of the 5-enolpyruvoylshikimate-3-phosphate synthase tetrahedral intermediate, *J. Biol. Chem. 265*, 5567−5572.
22. Daugherty, M., Vonstein, V., Overbeek, R., and Osterman, A. (2001) Archaeal shikimate kinase, a new member of the GHMP-kinase family, *J. Bacteriol. 183*, 292−300.
23. Lanzetta, P. A., Alvarez, L. J., Reinach, P. S., and Candia, O. A. (1979) An improved assay for nanomole amounts of inorganic phosphate, *Anal. Biochem. 100*, 95−97.
24. Kabsch, W. (1993) Automatic procession of rotation diffraction data from crystals of initially unknown symmetry and cell constrants, *J. Appl. Crystallogr. 26*, 795−800.
25. Brunger, A. T., Adams, P. D., Clore, G. M., DeLano, W. L., Gros, P., Grosse-Kunstleve, R. W., Jiang, J. S., Kuszewski, J., Nilges, M., Pannu, N. S., Read, R. J., Rice, L. M., Simonson, T., and Warren, G. L. (1998) Crystallography & NMR system: A new software suite for macromolecular structure determination, *Acta Crystallogr. B. 54*, 905−921.
26. Jones, T. A., Zou, J. Y., Cowan, S. W., and Kjeldgaard (1991) Improved methods for building protein models in electron density maps and the location of errors in these models, *Acta Crystallogr. B. 47*, 110−119.
27. Kraulis, P. J. (1991) MOLSCRIPT: a program to produce both detailed and schematic plots of protein structures, *J. Appl. Crystallogr. 24*, 946−950.
28. Merrit, E. A., and Bacon, D. J. (1997) Raster3D: Photorealistic Molecular Graphics, *Methods Enzymol. 277*, 505−524.
29. Esnouf, R. M. (1997) An extensively modified version of MolScript that includes greatly enhanced coloring capabilities, *J. Mol. Graph. Model. 15*, 132−134, 112−113.
30. Morris, G. M., Goodsell, D. S., Halliday, R. S., Huey, R., Hart, W. E., Belew, R. K., and Olson, A. J. (1998) Automated docking using a lamarckian genetic algorithm and an empirical binding free energy function, *J. Comput. Chem. 19*, 1639−1662.
31. Gasteiger, J., and Marsili, M. (1980) Iterative partial equalization of orbital electronegativity—A rapid access to atomic charges, *Tetrahedron 36*, 3219−3228.
32. Schonbrunn, E., Sack, S., Eschenburg, S., Perrakis, A., Krekel, F., Amrhein, N., and Mandelkow, E. (1996) Crystal structure of UDP−*N*-acetylglucosamine enolpyruvyltransferase, the target of the antibiotic fosfomycin, *Structure 4*, 1065−1075.
33. Skarzynski, T., Mistry, A., Wonacott, A., Hutchinson, S. E., Kelly, V. A., and Duncan, K. (1996) Structure of UDP−*N*-acetylglucosamine enolpyruvyl transferase, an enzyme essential for the synthesis of bacterial peptidoglycan, complexed with substrate UDP−*N*-acetylglucosamine and the drug fosfomycin, *Structure 4*, 1465−1474.
34. Schonbrunn, E., Svergun, D. I., Amrhein, N., and Koch, M. H. (1998) Studies on the conformational changes in the bacterial cell wall biosynthetic enzyme UDP−*N*-acetylglucosamine enolpyruvyltransferase (MurA), *Eur. J. Biochem. 253*, 406−412.
35. Eschenburg, S., and Schonbrunn, E. (2000) Comparative X-ray analysis of the un-liganded fosfomycin-target murA, *Proteins: Struct., Funct., Genet. 40*, 290−298.
36. Schonbrunn, E., Eschenburg, S., Luger, K., Kabsch, W., and Amrhein, N. (2000) Structural basis for the interaction of the fluorescence probe 8- anilino-1-naphthalenesulfonate (ANS) with the antibiotic target MurA, *Proc. Natl. Acad. Sci. U.S.A. 97*, 6345−6349.
37. Stauffer, M. E., Young, J. K., and Evans, J. N. (2001) Shikimate-3-phosphate binds to the isolated N-terminal domain of 5-enolpyruvylshikimate-3-phosphate synthase, *Biochemistry 40*, 3951−3957.
38. Eschenburg, S., Priestman, M. A., and Schonbrunn, E. (2005) Evidence that the fosfomycin target Cys115 in UDP−*N*-acetylglucosamine enolpyruvyl transferase (MurA) is essential for product release, *J. Biol. Chem. 280*, 3757−3763.

BI048198D